

# Non-linear effects from variable thermal conductivity and mantle internal heating: implications for massive melting and secular cooling of the mantle

A.P. van den Berg<sup>a,\*</sup>, D.A. Yuen<sup>b</sup>, J.R. Allwardt<sup>b,1</sup>

<sup>a</sup> *Department of Theoretical Geophysics, University of Utrecht, P.O. Box 80.021, 3508 TA Utrecht, The Netherlands*

<sup>b</sup> *Department of Geology and Geophysics, Minnesota Supercomputer Institute, University of Minnesota, Minneapolis, MN 55415-1227, USA*

Received 3 April 2001; received in revised form 12 October 2001; accepted 9 November 2001

## Abstract

The temperature-dependence of the phonon portion of the thermal conductivity  $k(T, P)$  devised by Hofmeister [Science 283 1699–1706] decreases with temperature, the same as in the dependence of mantle viscosity. Such a functional relationship of  $\partial k/\partial T < 0$ , when coupled with internal heating would present a situation very conducive for positive feedback action. On the other hand, the photon dependence of the conductivity has a functional relationship of  $\partial k/\partial T > 0$ . Thus, there can be a tradeoff between the phonon and photon contributions in the conductivity in the presence of internal heating. We have conducted two-dimensional calculations of mantle convection up to a surface Rayleigh number of around five million and an internal heating of chondritic abundance, with the extended-Boussinesq approximation in which the dissipation number has been set to 0.47 and depth-dependent thermal expansivity, decreasing by a factor of 5 across the mantle. The value of the constant mantle viscosity and the amount of internal heating are varied. For an enhanced radiative contribution [J. Geophys. Res. 84 (B4) 1603–1610] the radiative component of the thermal conductivity can exceed the phonon contribution in the upper mantle. Our results show that in all cases with basal heating the average mantle temperature of the variable conductivity models are higher than those of the corresponding constant conductivity models. But the interior thermal difference between the two conductivity models decreases (1) with greater vigor of convection, (2) an increase of internal heating and (3) an increase in the radiative contribution to the conductivity. The interior mantle temperature is significantly hotter, more than 500 °C, than the constant conductivity model, for the  $k(T, P)$  model with the less enhanced radiative component [Science 283 1699–1706]. These results would suggest that some sort of massive melting in the young earth might have occurred with  $k(T, P)$  and that there should not be so much radioactivity in the lower mantle today without incurring the wrath of some melting. We have also studied the effects of  $k(T, P)$  on slowing down the mantle secular cooling process by monitoring the gradual decrease in mantle temperature following an imposition of an adiabatic boundary condition at the core-mantle boundary. A decay time of 3.6 Gy has been taken for the mantle radioactivity and we have varied the initial amount of radioactive heating from chondritic value to four times the chondritic value. A significant delay in the cooling process of at least 1–2 Gy is found for a surface Rayleigh number of between  $5 \times 10^6$  to  $5 \times 10^7$ . The mantle temperature can be heated up by 300–400 °C for initial radiogenic heating value characteristic of the Archean. We find the strongest deviations from the constant conductivity case for a silicate model by Hofmeister [Science 283 1699–1706] and intermediate values for an enhanced radiative conductivity model comparable

\*Corresponding author. Tel.: +31-30-253-5072; fax: +31-30-253-5030.

E-mail address: berg@geo.uu.nl (A.P. van den Berg).

<sup>1</sup>Present address: Stanford University Department of GES, Building 320, Stanford, CA 94305, USA.

to the model of Shankland et al. [J. Geophys. Res. 84 (B4) 1603–1610]. Such high mantle temperatures maintained for a long time by variable thermal conductivity would have important consequences on the thermal and petrological evolution of the mantle. © 2002 Elsevier Science B.V. All rights reserved.

*Keywords:* Mantle convection; Thermal conductivity; Secular cooling

## 1. Introduction

The time-dependent equation governing the thermal evolution in mantle convection has thermal conductivity as one of the transport coefficients. This physical parameter is commonly assumed to have constant property for the entire mantle. Yet other physical parameters in mantle convection, such as viscosity (Weertman, 1970) and thermal expansivity (Chopelas and Boehler, 1992), vary with temperature and pressure and variations in these properties can change the style of mantle convection (e.g. Christensen and Yuen (1985), Hansen et al. (1993)). A temperature-dependent thermal conductivity would endow the temperature diffusion equation with a strongly non-linear character (e.g. Barenblatt and Zel'dovich (1972)), which makes it very different from a linear thermal diffusion equation (Barenblatt, 1996). More than four decades ago both (Lubimova, 1958) and (Mac Donald, 1959) embarked in pioneering studies on the thermal evolution of the earth by solving numerically the formidable non-linear temperature equation due to the usage of a strong radiative term in the thermal conductivity. However, in the intervening years of plate tectonics the role of variable thermal conductivity in mantle convection has gone unappreciated for many years until the recent model based on solid-state physics of phonons and infrared spectroscopy (Hofmeister, 1999). In the past year there have been initial studies on the role played by variable conductivity on various aspects of mantle dynamics, ranging from slab problems (Hauck et al., 1999), sedimentary basin formation (Starin et al., 2000), oceanic heat flow and seafloor topography (Honda and Yuen, 2001) mantle convection in both time-dependent three-dimensional situations (Dubuffet et al., 1999, 2000; Dubuffet and Yuen, 2000) and steady-state two-dimensional models (van den Berg et al., 2001) and shear-zone formation (Branlund et al., 2000). This present work focuses on the non-linear interaction between mantle internal heating, which increases

mantle temperature, and temperature-dependent thermal conductivity.

From solid-state physics it is well-known that the temperature-dependence of thermal conductivity based on phonon transport decreases with increasing temperature due to greater collision frequency (e.g. Klemens (1958), Ross et al. (1984)). Besides the usual  $1/T$  dependence from phonon collisions, there is also an exponential dependence on  $T$ , due to volumetric changes from the thermal pressure. This induces an exponential decrease of  $k(T)$  with increasing temperature as  $\exp(-CT)$ , with  $C$  depending on the product of both the Grueneisen parameter and the thermal expansivity. This would mean that the temperature derivative  $\partial k/\partial T$ , would be a negative quantity, in contrast to radiative heat-transfer by photons (Siegel and Howell, 1972), which has  $\partial k/\partial T$  positive. The negative nature of  $\partial k/\partial T$  in the phonon conductivity would lead to a distinct possibility of positive feedback with internal heating. Since an increase of temperature due to local heat production, be it viscous dissipation or internal heating, would lead to a decrease in the local thermal conductivity, the local temperature would increase due to the trapped heat, thus inducing the prospects for the development of positive feedback. Branlund et al. (2000) have shown that such a positive feedback can take place in the feedback between the localized heat generated by viscous dissipation and variable conductivity, which results in a reduction of the timescales for thermal instability to occur in shear-zone formation. Besides the phonon contribution to the conductivity, it would also be interesting to study the dynamical effects arising from the enhanced radiative conductivity model of Shankland et al. (1979), since van den Berg et al. (2001) already found the interesting paradoxical result that enhanced radiative contribution would produce a higher surface heatflow, as compared to both the constant conductivity model and the Hofmeister (1999) variable conductivity model. The purpose of this paper is to examine the possibilities for enhanced heating in the mantle

by the interaction between variable conductivity and radiogenic heating and to evaluate the difference between the variable and constant conductivity models, for which Leitch and Yuen (1989) have already delineated the conditions for melting in the mantle from various amounts of internal heating. This was conducted in a compressible model, where mechanical heating contributions from adiabatic compression and viscous dissipation are included. The second aim of this paper is to investigate the influence of variable conductivity on secular cooling of the mantle, since we would expect a hindrance to the cooling process by the prospects of a positive feedback between variable  $k$  because of its dependence on the temperature and internal heating, which raises the temperature. All previous works on transient secular cooling of the mantle (Daly, 1980; Quarenì et al., 1985; Choblet and Sotin, 2000) have been based on constant thermal conductivity.

We begin by going over the thermal conductivity and the numerical models. Then we discuss the results pertaining to the difference in the interior temperature between constant and variable conductivity models for various amounts of radiogenic heating. The issue of secular cooling in the presence of variable conductivity will be taken up next for various amounts of radiogenic heating and different convective strengths. Finally, we discuss the implications of our results and give the concluding remarks.

## 2. Thermal conductivity and numerical models

### 2.1. Thermal conductivity

The thermal conductivity used here is based on the model by Hofmeister (1999). This model is semi-empirically based on spectroscopy and combines conductivity contributions from both lattice vibrations (phonon part) and from radiative (photon) transport. It takes the form

$$k(T, P) = k_0 \left( \frac{298}{T} \right)^a \exp \left[ - \left( 4\gamma + \frac{1}{3} \right) \alpha (T - 298) \right] \times \left( 1 + \frac{K'_0 P}{K_0} \right) + f \sum_{i=0}^3 b_i T^i \quad (1)$$

The physical parameter values in dimensional form are given in Table 1.

The model case where the prefactor of the radiative term  $f = 1$  and  $b_i$  as listed in Table 1 corresponds the Hofmeister (1999) model. We also considered model cases with an enhanced radiative contribution with a larger value of  $f = 4.7$ , thus mimicking the Shankland conductivity model, which has a significant radiative contribution for olivine in the upper mantle (Shankland et al., 1979). We regard this as an end-member in the radiative transfer family. Radiative transfer may also be enhanced for increasing amounts of iron in the deep lower mantle (Manga and Jeanloz, 1996). This same conductivity model with  $f = 4.7$  has been applied in an investigation of steady-state mantle heat-transfer for the whole mantle (van den Berg et al., 2001). From the functional form of  $k(T, P)$  one can show easily that there exists a low conductivity zone (LCZ) at a depth between 100 and 150 km for the Hofmeister conductivity model with  $f = 1.0$  for a representative geotherm taken from oceanic boundary layer cooling (e.g. Parsons and Sclater (1977)). Although the pressure dependence of  $k(p, T)$  increases the conductivity more than  $T$  to decrease it in the Hofmeister model, it is the formation of a LCZ, which governs the formation of hot material under the lithosphere. As we show in Section 2.2, this LCZ plays an important role in delaying the secular cooling of the mantle.

### 2.2. Numerical model

We use an infinite Prandtl number model for an incompressible isoviscous internally heated fluid with temperature and pressure dependent thermal conductivity and depth dependent thermal expansivity, which decreases by a factor of 5 across the mantle (van den Berg and Yuen, 1998). We apply the extended Boussinesq approximation (Steinbach et al., 1989; Ita and King, 1994), which includes both adiabatic heating and viscous dissipation. The equations have been non-dimensionalized using the following scaling parameters, where symbols and parameter values are defined in Table 1, spatial scale,  $x_0 = h$  the depth of the two-dimensional rectangular domain, time scale,  $t_0 = h^2/\kappa_0$  a thermal diffusion time for

Table 1  
Physical parameters

Symbol	Definition	Value
$h$	Height of the domain	$3 \times 10^6$ m
$z$	Depth coordinate aligned with gravity	–
$P$	Static pressure	–
$\Delta p$	Dynamic pressure	–
$T$	Temperature	–
$\Delta T$	Temperature scale value	3500 K
$u_i$	Velocity field component	–
$e_{ij} = \partial_j u_i + \partial_i u_j$	Strain rate tensor	–
$e = [1/2 e_{ij} e_{ij}]^{1/2}$	Second invariant of strain rate	–
$w$	Vertical velocity aligned with gravity	–
$\eta$	Uniform viscosity	–
$\tau_{ij} = \eta e_{ij}$	Viscous stress tensor	–
$\Phi = \eta e^2$	Viscous dissipation function	–
$\alpha(z) = \Delta\alpha/[c(1-z) + 1]^3$	Depth dependent thermal expansivity	–
$\Delta\alpha = \alpha(0)\alpha(1)$		5
$c = \Delta\alpha^{1/3} - 1$		–
$\alpha_0$	Thermal expansivity scale value	$2 \times 10^{-5}$ K <sup>-1</sup>
$\rho$	Density	–
$\rho_0$	Density scale value	4000 kg/m <sup>3</sup>
$C_p$	Specific heat	1250 J/K/kg
$k$	Thermal conductivity	–
$k_0$	Conductivity scale value	4.7 W/m/K
$a$	Conductivity power-law index	0.3
$\gamma$	Grueneisen parameter	1.2
$K_0$	Bulk modulus	261 GPa
$K'_0$	Pressure derivative of bulk modulus	5
$b_0$	Coefficient phonon conductivity	$1.7530 \times 10^{-2}$
$b_1$		$-1.0365 \times 10^{-4}$
$b_2$		$2.2451 \times 10^{-7}$
$b_3$		$-3.4071 \times 10^{-11}$
$\kappa = k/\rho C_p$	Thermal diffusivity	–
$g$	Gravitational acceleration	9.8 m/s <sup>2</sup>
$H(t) = H_0 \exp(-t/\tau)$	Time-dependent internal heating	(W/kg)
$\tau$	Dimensional decay time of radioactive heating	3.6 Gy
$H_0$	Dimensional value of internal heating	(W/kg)
$R = H_0 h^2 / C_p \kappa_0 \Delta T$	Non-dimensional internal heating number	–
	$R = 10 \Leftrightarrow H_0 = 4.6 \times 10^{-12}$ W/kg	
$Ra = \rho_0 \alpha_0 g \Delta T h^3 / \kappa_0 \eta_0$	Rayleigh number	–
$Di = \alpha_0 g h / C_p$	Dissipation number	0.47

the whole layer depth. The temperature scale is the temperature contrast  $\Delta T$  between top and bottom boundary in the models with prescribed bottom temperature.

The model equations expressing conservation of mass (Eq. (2)), momentum (Eq. (3)), and energy (Eq. (4)) are

$$\partial_j u_j = 0 \quad (2)$$

$$-\partial_i \Delta p + \partial_j \tau_{ij} = \alpha Ra T \delta_{i3} \quad (3)$$

$$\frac{DT}{Dt} = \partial_j \kappa \partial_j T + \alpha Di w (T + T_0) + \frac{Di}{Ra} \Phi + RH(t) \quad (4)$$

They are applied to a situation with both basal and internal heating. The notations for the temperature, deviatoric stress, dynamical pressure, viscous heating and other symbols are provided in Table 1. In Eq. (4)  $D/Dt$  denotes the substantive derivative. The individual terms on the right-hand side of Eq. (4) are related

to heat conduction, adiabatic heating, viscous heating and internal heating from radiogenic heat sources respectively. The first term in the right-hand side of Eq. (4), written in a conservative form appropriate for finite elements, contains the pressure and temperature dependent thermal diffusivity  $\kappa = k(T, P)/(\rho C_p)$ . The temperature dependence in the variable  $k$  model used represents a non-linearity in the energy equation. We note that there are three non-linear terms present in the divergence of the heat flux vector (e.g. Dubuffet et al. (1999), van den Berg et al. (2001)). We note that we have not considered phase transitions here, which would yield jumps in the thermal conductivity.

We have applied finite element methods to solve Eqs. (2)–(4), (van den Berg et al., 1993). The continuity Eq. (2) is satisfied in an approximate way by the use of a penalty function method for the Stokes equation (Hughes, 1987) with a penalty parameter value  $\epsilon = 10^{-6}$ . The resulting system of equations can be written as,

$$SU = F(T) \quad (5)$$

$$M \frac{dT}{dt} = A(T, U)T + G(U) \quad (6)$$

where  $S$ ,  $M$  and  $A$  are finite element matrices and represent the viscous rheology, thermal inertia and thermal advection and adiabatic heating contributions, respectively, and  $F$  and  $G$  are right-hand side vectors and denote the buoyancy and viscous heating terms. The stiffness matrix  $A$  of Eq. (6) contains contributions from the conduction and convection terms and also from the adiabatic compression term in Eq. (4). The temperature dependent conductivity in the non-linear diffusion term has entered in the stiffness matrix  $A$  of Eq. (6). The vector  $G$  on the right-hand side contains contributions from internal heating, viscous dissipation and adiabatic compression.

The discretized Eqs. (5) and (6) are integrated in time as a set of ordinary differential equations using a predictor–corrector (PC) scheme where the non-linear diffusion term can be linearized in the corrector part of the algorithm. A detailed description of the algorithm is given in the Appendix A. Besides the PC scheme we have also used a fully implicit time integration method with a large timestep (two times the Courant timestep) for obtaining rapidly statistically steady-state solutions.

We have used a two-dimensional Cartesian model with an aspect ratio of 2.5. and a depth of 3000 km. Quadratic six-point triangular finite elements were used for the velocity field with a subdivision of each velocity element into four linear temperature elements (van den Berg et al., 1993). The finite element code used is based on the SEPRAN finite element package (<http://dutita0.twi.tudelft.nl/sepran/sepran.html>). The finite element mesh contained up to  $200 \times 200$  nodal points with local refinement near the horizontal boundaries. Impermeable free slip mechanical boundary conditions were used on all boundaries. For the thermal boundary conditions we imposed a temperature of  $0^\circ\text{C}$  centigrade at the top surface and zero heatflux along the vertical boundaries. For the bottom boundary we used either a prescribed temperature, when computing a statistically thermal equilibrium state or a zero heat flux or adiabatic boundary condition in the computations for models subject to secular cooling. In the first model case constant internal heating was used. For the secular cooling models we have applied a radioactive heat source with a decay time value of 3.6 Gy. We note here that the equations have been non-dimensionalized but we will present the results in dimensional form because of the nature of the thermal conductivity equation, which necessitates one to impose a certain temperature for the core–mantle boundary, which is set to 3773 K in this study.

### 3. Results

#### 3.1. Combined influence on mantle temperature from internal heating, mechanical heating and variable thermal conductivity

It is well established that internal heating in compressible mantle convection can enhance the propensity toward localized overheating in the mantle (Machetel and Yuen, 1989; Leitch and Yuen, 1989; Zhang and Yuen, 1996) much more so than in Boussinesq models. This has also shown to be the case for thermal-chemical convection with the extended-Boussinesq approximation (Hansen and Yuen, 2000). In Fig. 1 we show a comparison at a low surface Rayleigh number of  $1.6 \times 10^5$  of the temperature fields between constant (left column) and variable (right column) thermal conductivity with

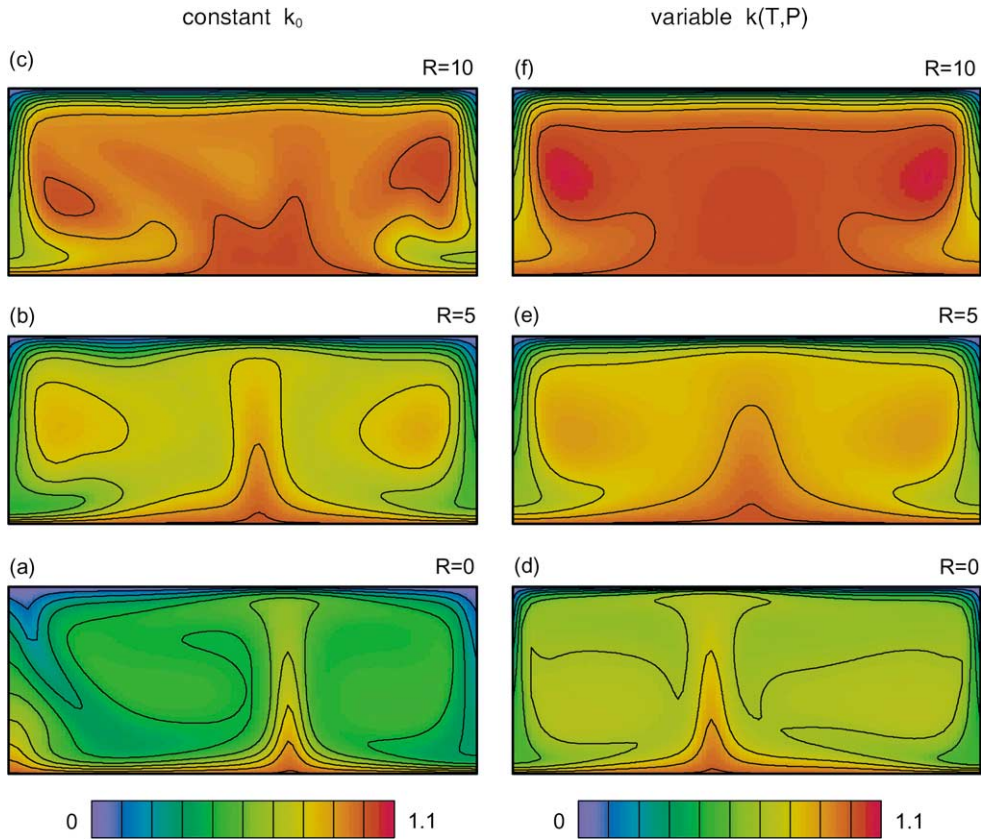


Fig. 1. Temperature field of statistically steady states for different model cases with surface Rayleigh number  $Ra_s = 1.6 \times 10^5$  and increasing internal heating from  $R = 0$  to 10 from bottom to top. Constant conductivity cases (a)–(c); variable conductivity cases (d)–(f). The  $f$ -value in the radiative conductivity term is 4.7.

$f = 4.7$ . All other physical properties and the thermal boundary conditions are the same with the exception of the thermal conductivity, which is the prime focus of this paper. Internal heating values ranging from no internal heating,  $R = 0$ , (bottom row) to roughly chondritic abundance,  $R = 10$ , are used. We note that the dimensionless parameter  $R$  for a bi-modal heating situation also contains both the internal heating rate from radioactivity and the scale value of the thermal conductivity  $k_0$  (Leitch and Yuen, 1989), taken here as the surface value of  $4.7 \text{ W/(m K)}$ .

These temperature fields are obtained after an integration time longer than the age of the earth and have been verified to be in a statistically equilibrated state. For the  $k(T, P)$  model we have used the enhanced radiative model with  $f = 4.7$  and the phonon

portion taken from the Hofmeister (1999) model. The temperature has been normalized with respect to a dimensionless value of 1.1 or 3850 centigrade. The surface heat flow is greater for the case of variable thermal conductivity by around 20%, consistent with the steady-state work in an aspect-ratio one box for Boussinesq convection with variable thermal conductivity (van den Berg et al., 2001). We can easily discern the higher temperatures attained by the variable conductivity case over the constant conductivity model. This temperature difference decreases with greater amount of internal heating because of the enhanced radiative contribution ( $f = 4.7$ ) in the conductivity, which attains a high value in the upper mantle (Fig. 6).

For a higher surface Rayleigh number at a  $Ra_s$  of  $2.6 \times 10^6$  and the strength of internal heating  $R$

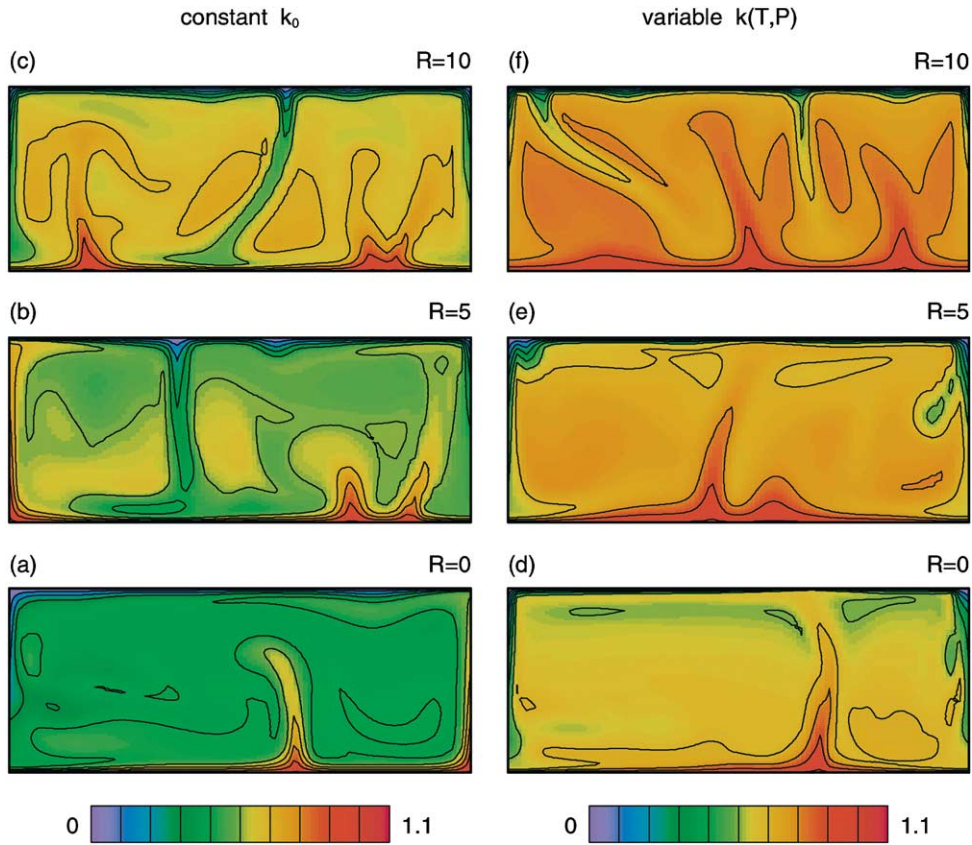


Fig. 2. Temperature fields for the same  $f$ -values as in Fig. 1 but for surface Rayleigh number  $2.6 \times 10^6$ .

increasing from 0 to 10, the mantle remains persistently much hotter by at least 300–400 °C, as shown in Fig. 2. The downwellings are much weaker for the variable conductivity cases, supporting the findings of Dubuffet et al. (2000) for a basal heating situation. The upwellings are broader in the case of variable conductivity, reminiscent of the work by Matyska et al. (1994), who employed a purely radiative thermal conductivity. Extrapolating these findings to a  $Ra_s$  of  $10^8$  we find that the temperature difference in the case for  $R = 10$  would still be at least 100–150 °C. However, the amount of internal heating in the Hadean and Archean is at least a factor of 4 greater (or  $R > 50$ ) from both the remnant heat from core formation and greater amount of radioactivity present in a young mantle. On these grounds, we may expect a substantial temperature difference between constant and variable conductivity models in the distant geological

past, when the surface Rayleigh number was higher than today's value because of the lower interior viscosity.

Figs. 3 and 4 display the one-dimensional profiles of the horizontally averaged temperature fields corresponding respectively to the two-dimensional thermal fields in Figs. 1 and 2. These averaged profiles delineate more conspicuously the much hotter mantle associated with variable thermal conductivity. There are relatively little differences, about 35 °C, between two- and three-dimensional averaged temperature profiles (Dubuffet et al., 2000). We note that for the higher surface Rayleigh number case with a chondritic abundance of radiogenic heating  $R = 10$  the rise in the temperature from the constant to the variable conductivity model is around 400 °C. The difference in the interior temperature between the variable and constant conductivity models decreases with larger amounts

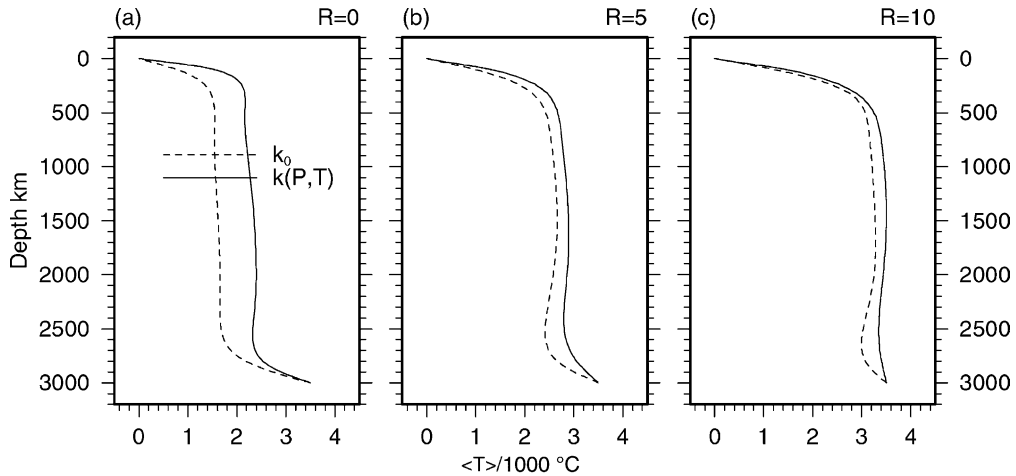


Fig. 3. Horizontally averaged temperature profiles for the three internal heating modes in Fig. 1 ( $Ra_s = 1.6 \times 10^5$ ). Dashed lines are for constant conductivity and the solid lines are for variable conductivity with  $f = 4.7$ .

of internal heating, due to the enhanced contribution from the radiative conductivity in the upper mantle. In Fig. 5, we show for the variable conductivity with  $f = 4.7$  the volumetrically averaged temperature  $\langle T \rangle$  for various amounts of internal heating and for surface Rayleigh numbers spanning 2 orders in magnitude. Leitch and Yuen (1989) have constructed a similar domain diagram for constant conductivity. The averaged temperature increases with larger internal heating  $R$

and decreases with increasing surface Rayleigh number ( $Ra_s$ ). However, it would still take a very vigorous convection, at  $Ra_s$  greatly exceeding  $10^8$  to bring the averaged interior temperature to a reasonable value of around 2300 K in the case of variable thermal conductivity. Choblet and Sotin (2000) have argued for a speed up in the convective readjustment process due to strongly temperature-dependent viscosity within the framework of a Boussinesq model without any

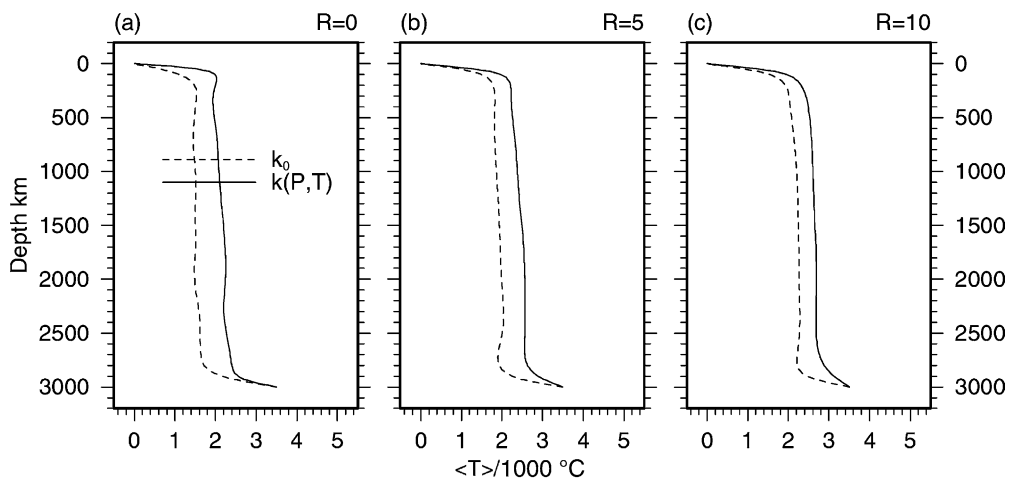


Fig. 4. Similar temperature profiles as in Fig. 3 but for the temperature fields of Fig. 1 corresponding to a surface Rayleigh number  $Ra_s = 2.6 \times 10^6$ . Dashed lines are for constant conductivity and the solid lines are for variable conductivity with  $f = 4.7$ .

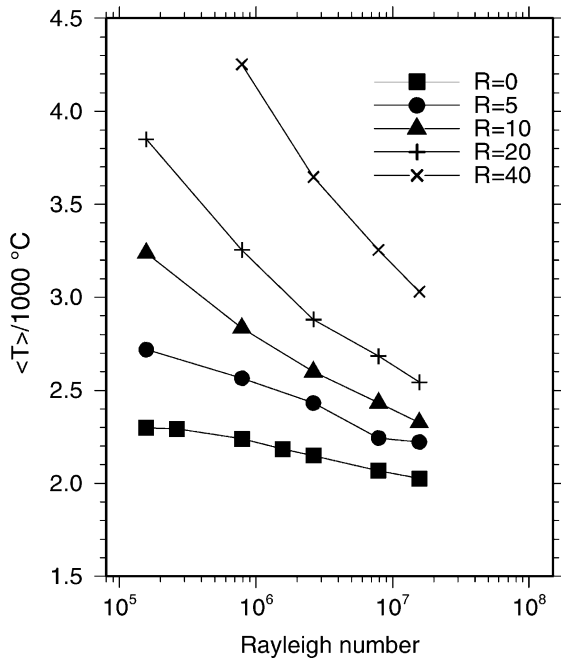


Fig. 5. Volume averaged temperature of statistically steady-state convection models with variable conductivity and a value of  $f = 4.7$  vs. the surface Rayleigh number for the internal heating modes  $R = 0, 5, 10, 20, 40$ . The first and fifth point of the bottom three curves corresponds to the temperature fields shown in Figs. 1 and 2 respectively.

mechanical heating effects. However, there has been no work done on the effects of variable viscosity on compressible convection for us to predict right now with much confidence the effects of variable viscosity on convective cooling at high surface Rayleigh number where mechanical heating effects, such as viscous dissipation, would also be enhanced (Balachandrar et al., 1993). Moreover, the pressure-dependent effects of mantle viscosity and thermal expansivity would also slow down convective vigor in the lower mantle (Hansen et al., 1993; van den Berg and Yuen, 1998) and allow heat to build up locally.

In Fig. 6 we diagnose the effects of the enhanced radiative conductivity ( $f = 4.7$ ) by comparing the results with the Hofmeister radiative conductivity ( $f = 1.0$ ) for various amounts of internal heating up to  $R = 40$ , corresponding to the amount of radiogenic heating during the Archaean epoch. Reducing the radiative component, as in the Hofmeister model, increases

tremendously the overall interior temperature for high values of internal heating ( $R > 20$ ).

This can be explained by the lower contribution of the radiative component, which does not bring about as efficient heat transfer as for the higher radiative contribution ( $f = 4.7$ ). This phenomenon can be observed in Fig. 6(d) and (b), where the thermal conductivity profiles have been decomposed into the radiative  $k_{\text{rad}}$ , the lattice  $k_{\text{lat}}$  contribution and the overall conductivity  $k_{\text{eff}}$ . What is remarkable is the dominance of the radiative contribution over the phonon contribution  $k_{\text{lat}}$  in the upper mantle for  $f = 4.7$  because of the feedback between internal heating and  $\partial k / \partial T > 0$ , which enhances heat transfer in the upper mantle and produces a cooler upper mantle. We note that the conductivity values in the lower mantle attained by the model with  $f = 4.7$  fall within the same range, 10–12 W/(m K), as those estimated according to mineral physics by Brown (1986) and to boundary-layer theory by Leitch (1995). Without the radiative boost provided by the higher  $f$ -value, there is a greater buildup of heat in the Hofmeister model (Fig. 6(c) and (d)), where we can clearly see the higher interior temperatures above the profiles associated with enhanced radiative conductivity (Fig. 6(a) and (b)). We note that there is a pronounced LCZ in the upper mantle developed from the Hofmeister model, while this LCZ is much weaker and concentrated in the extremely shallow portion of the upper mantle for the enhanced radiative conductivity ( $f = 4.7$ ) case.

The results presented in this section show definitely the greater proclivity of the mantle to melting situations because of the higher interior temperatures, when variable thermal conductivity, especially with  $f = 1.0$ , is included in the convection model. We have used the case for  $f = 4.7$  as an upper bound for the effects of radiative heat transfer. We note that this radiative conductivity model presented by Shankland et al. (1979) was for a pure olivine upper mantle. Hence, it is likely an overestimate for a dirtier real whole mantle containing less transparent phases and opaque pieces, which would decrease the transparency and lower the radiative conductivity from the upper bounds of the model with  $f = 4.7$ . If anything, the most probable hypothesis may be that  $k_{\text{rad}}$  very likely peaks somewhere in the upper mantle and decreases below in the lower mantle. But more laboratory work is necessary in this direction.

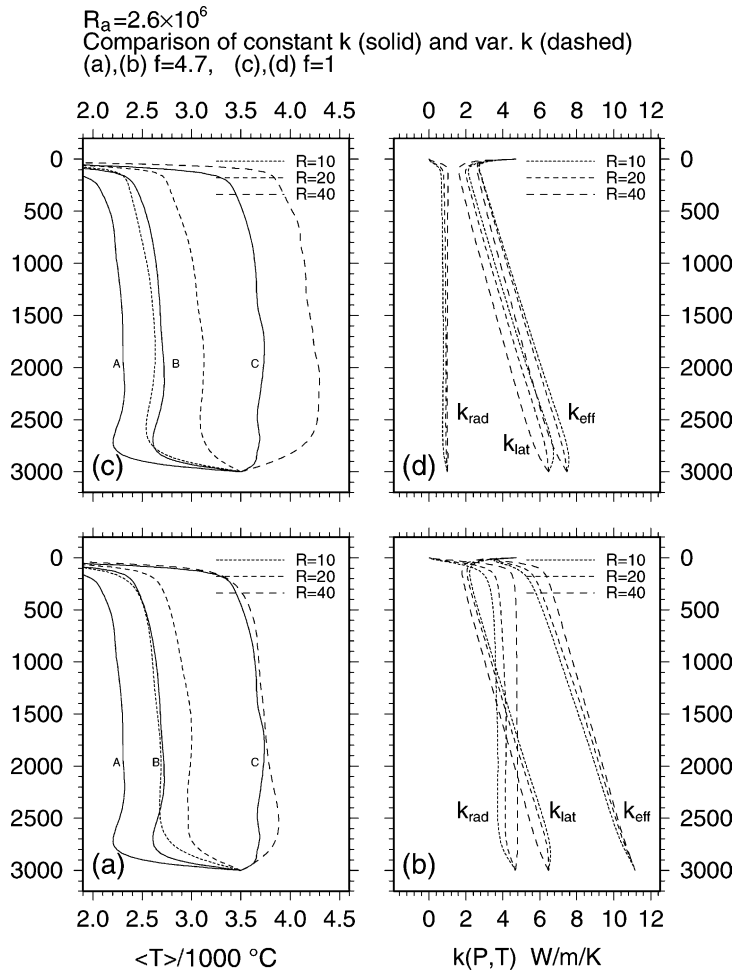


Fig. 6. Temperature and thermal conductivity profiles for two different radiative conductivity models ( $f = 1.0$  and  $4.7$ ) and various values of internal heating  $R = 10, 20, 40$ . The surface Rayleigh number is  $Ra_s = 2.6 \times 10^6$ . Solid curves denote results from constant thermal conductivity. The thermal conductivity profiles have been decomposed into the phonon  $k_{\text{lat}}$  and the radiative  $k_{\text{rad}}$  components. A, B, C are symbols representing  $R = 10, 20, 40$ , respectively, for constant thermal conductivity, while the dashed curves represent results from variable conductivity. See symbols in the panels for the amount of internal heating.

### 3.2. Effects of variable thermal conductivity on secular cooling

In this section we will examine the consequences of variable thermal conductivity on the transient cooling process in the mantle, because of its potentially important implications on mantle thermal evolution in non-equilibrium circumstances involving heat-exchange between the core and mantle (Steinbach et al., 1993).

The situation we consider is much simpler in that an adiabatic (zero heat flux) boundary condition is imposed at the bottom boundary or the core-mantle boundary. We have employed the same initial condition for all of the cases examined. This initial condition comes from a long-term statistically equilibrated solution, which was derived for an internally heated, variable conductivity case with a constant internal heating set to  $R = 40$ , a surface Rayleigh number  $Ra_s = 8 \times 10^6$  and a  $k(T, P)$  conductivity model with

$f = 4.7$ . We then switch on to a time-dependent internal heating at  $t = 0$ , in dimensional form specified as  $H(t) = H_0 \exp(-\lambda t)$ , where the exponential-folding time for radioactive decay,  $1/\lambda$ , is set to 3.6 Gy, corresponding to a half-life time of 2.5 Gy.

We show the time histories of the volumetrically averaged temperature  $\langle T \rangle$  as a function of time for three different radiogenic heating rates  $R = 10, 20$  and 40 and for two different  $Ra_s$ ,  $8 \times 10^6$  (Fig. 7) and  $1.6 \times 10^7$  (Fig. 8). Three thermal conductivity models have been employed. Besides the constant conductivity case (labeled  $k_0$ ) and the enhanced photon thermal

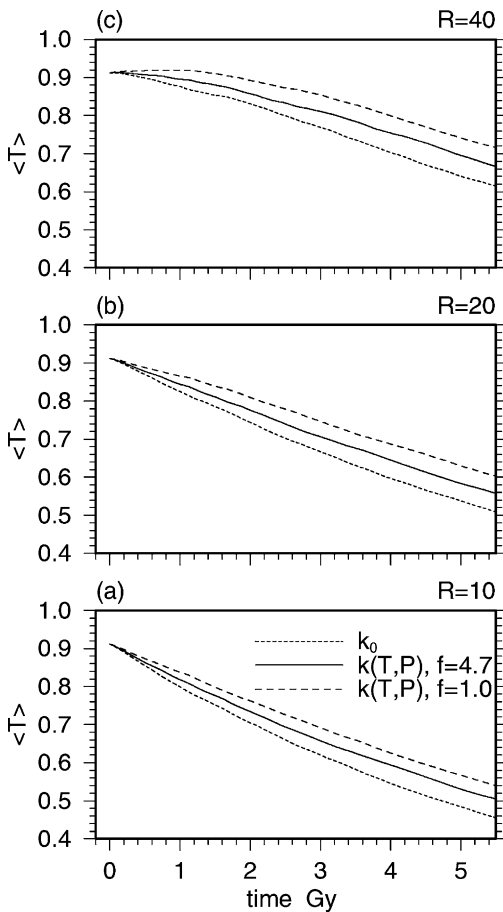


Fig. 7. Volume averaged temperature versus dimensional time for surface Rayleigh number  $Ra_s = 8 \times 10^6$  and three internal heating strengths  $R = 10, 20, 40$ . Dotted curves are for constant conductivity, dashed curves for the conductivity model by Hofmeister (1999) and the solid lines are for a conductivity model with 4.7 times enhanced radiative component.

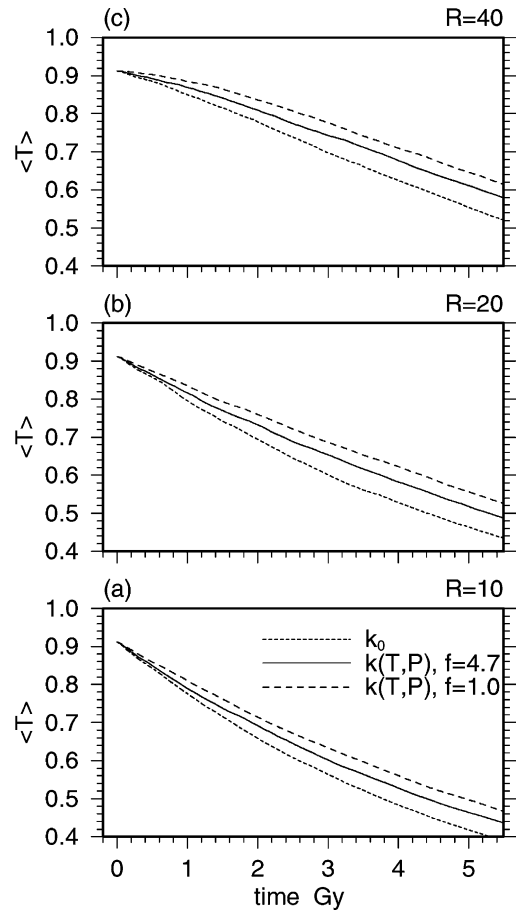


Fig. 8. Volume averaged temperature versus dimensional time for surface Rayleigh number  $Ra_s = 1.6 \times 10^7$  and three internal heating magnitudes  $R = 10, 20, 40$ . Dotted curves are for constant conductivity, dashed curves ( $f = 1.0$ ) for the conductivity model by Hofmeister (1999) and the solid lines are for a conductivity model with 4.7 times enhanced radiative component.

conductivity ( $f = 4.7$ ), we have also considered the original Hofmeister model with a more modest radiative contribution ( $f = 1.0$ ). In all the cases, the mantle cools the fastest with a constant thermal conductivity. There is a delay in the cooling in the variable conductivity models, with the Hofmeister ( $f = 1.0$ ) model producing the most impact. This can be explained by the existence of a LCZ or conductivity minimum in the upper mantle in the Hofmeister conductivity model ( $f = 1.0$ ) (Hofmeister, 1999) and the near absence of a LCZ in the conductivity model with greater radiative contribution ( $f = 4.7$ ). This zone of low

conductivity near the thermal boundary acts to trap the heat there and inhibits the cooling process at the top thermal boundary layer. The global convective vigor, as measured by the time-averaged RMS velocity also shows that convection with variable conductivity is

weaker than that with constant conductivity. Table 2 compares the two models for  $Ra_s = 8 \times 10^6$  and two different rates of internal heating. We see that  $v_{RMS}$  is smaller for variable conductivity. The smaller convective vigor in variable conductivity convection may

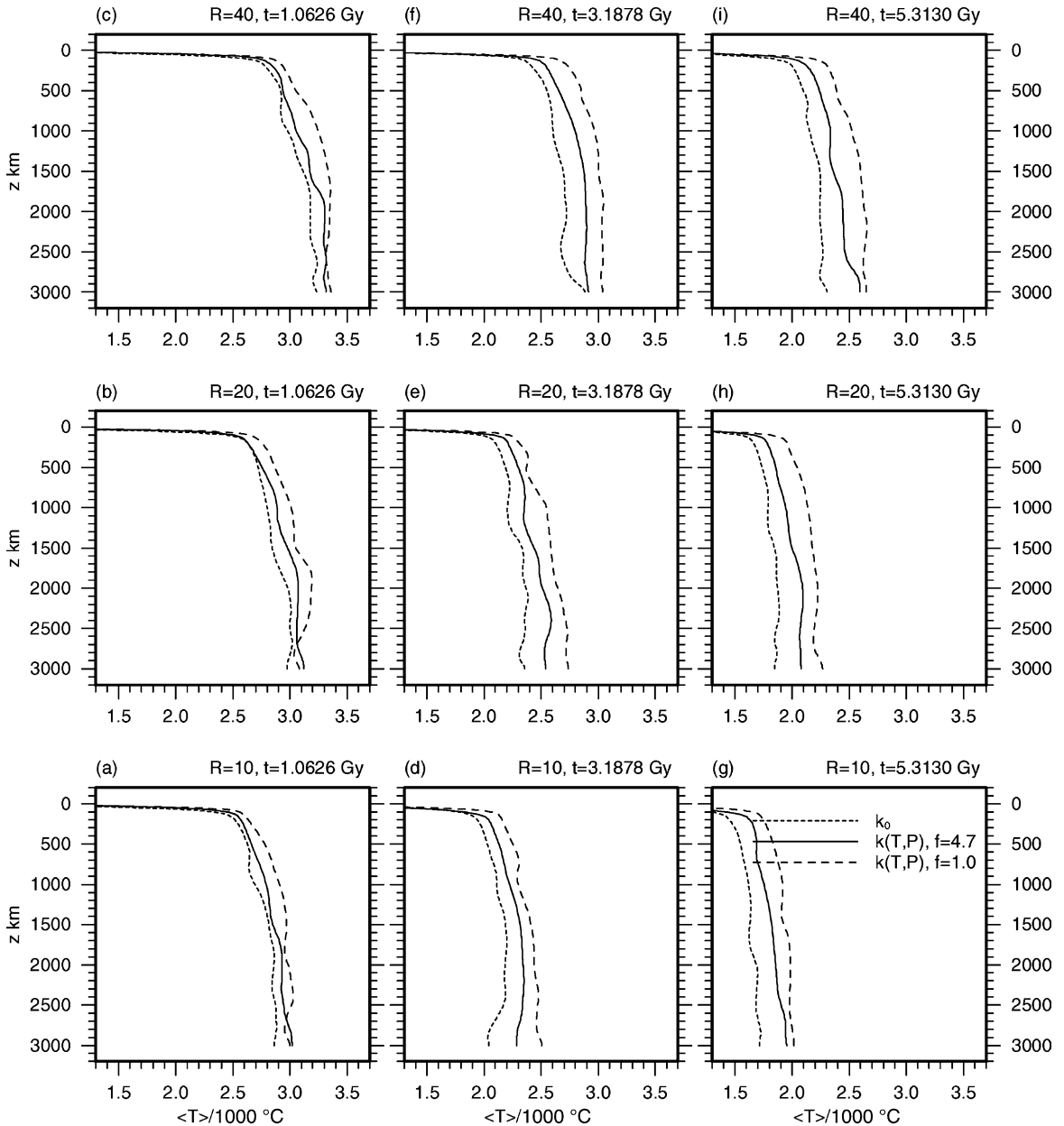


Fig. 9. Horizontally averaged temperature profiles of temperature snapshots for the cases shown in Fig. 7, for surface Rayleigh number  $Ra_s = 8 \times 10^6$ . Dimensional snapshot time values are at 1.06 Gy (a–c) 3.19 Gy (d–f) and 5.31 Gy (g–i).

Table 2  
Time averaged RMS velocity in cm per year

$k$ model	$R = 10$	$R = 40$
$k_0(\text{constant})$	0.695	0.793
$k(T, P), f = 1$	0.654	0.728

be responsible for the delay in the cooling rate. This preliminary scan of this global trend should be investigated further with more local analysis, addressing the differences between the upwellings and the downwellings.

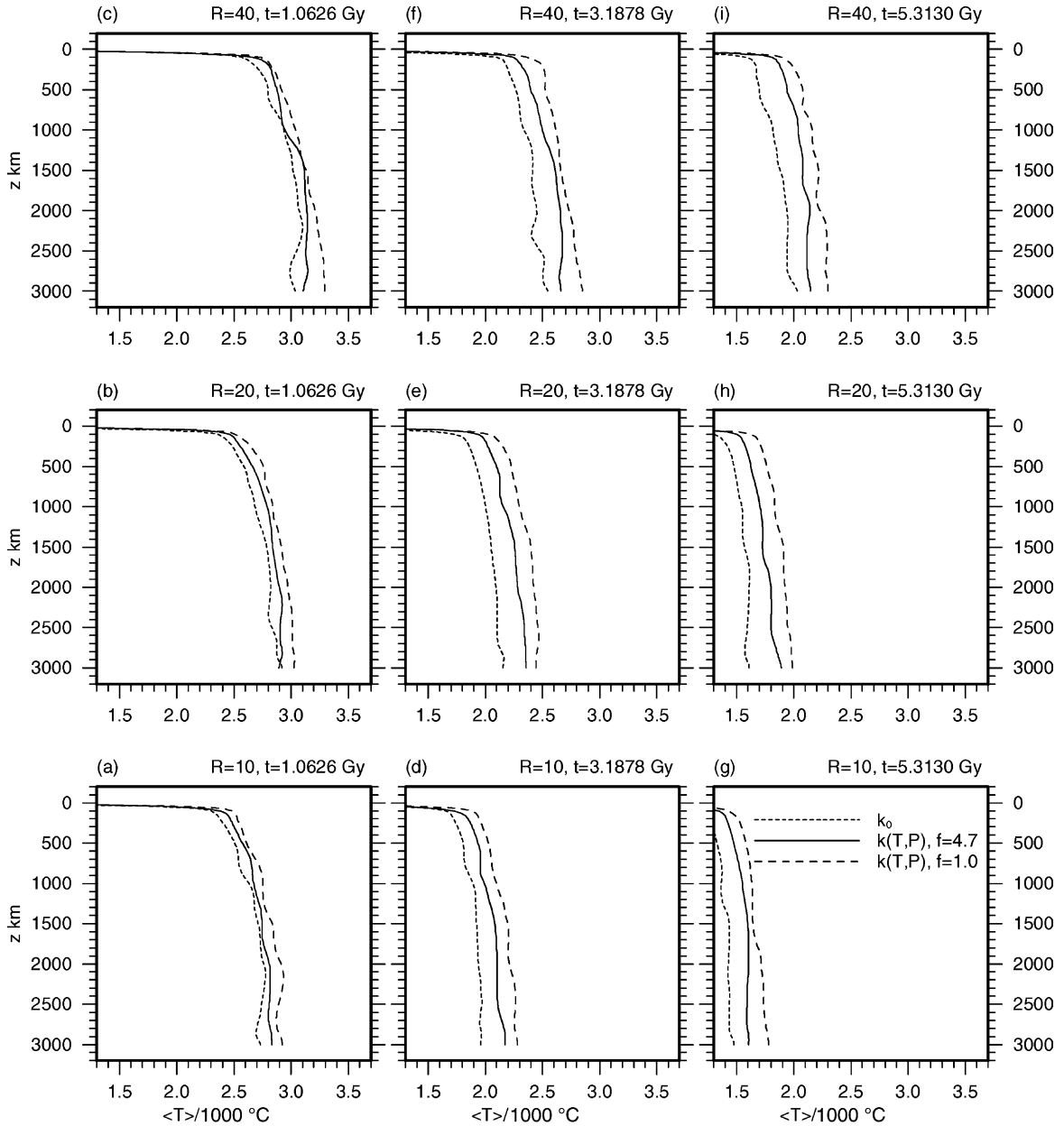


Fig. 10. Horizontally averaged temperature profiles of temperature snapshots for the model cases shown in Fig. 8, for surface Rayleigh number  $Ra_s = 1.6 \times 10^7$ . Dimensional snapshot time values are at 1.06 Gy (a–c) 3.19 Gy (d–f) and 5.31 Gy (g–i).

The cooling rate is impeded with greater amounts of internal heating and is accelerated with higher  $Ra_s$  (Fig. 8), which is well-known from constant conductivity results (e.g. Daly (1980), DeLandro-Clarke and Jarvis (1997)).

Rather large differences in  $\langle T \rangle$ , of the order of several hundred degrees, are found between the constant and variable conductivity models. Using  $\langle T \rangle = 0.7$  as a level, we can estimate a delay time of around 1 Gy for  $Ra = 8 \times 10^6$  and 10. For higher values of  $R$ , like 40, which would be more realistic for the Archean period, the delay times for the level of  $\langle T \rangle$  to be reached is substantially lengthened by a factor close to 2 for  $R = 40$  and  $Ra_s = 8 \times 10^6$ . Thus, both internal heating and variable conductivity act in concert to keep the mantle hot, especially with the LCZ for the Hofmeister conductivity model, thus leading to some interesting scenarios to be discussed below.

In Figs. 9 and 10 we show the temporal evolution of the horizontally averaged temperature profiles of the cases for  $\langle T \rangle$  displayed respectively in Figs. 7 and 8. From these temperature profiles emerge two salient points: (1) much higher temperatures are maintained by the Hofmeister conductivity model at all depths because of the presence of the poignant LCZ; (2) thermal differences of at least  $400^\circ\text{C}$  persist for a length of time in excess of the age of the earth for a surface Rayleigh number of  $1.6 \times 10^7$  and realistic initial radiogenic heating rates for a young earth.

## 4. Discussion and concluding remarks

### 4.1. Overheating in the mantle

Our results show that there is a large increase in the interior mantle temperature by at least  $300\text{--}400^\circ\text{C}$ , as a consequence of the various non-linear interactions between internal heating and variable thermal conductivity. There are such possibilities because of the two competing conductivity mechanisms phonon and radiative which can cause changes in the sign of  $\partial k/\partial T$ .

From Fig. 1 and 2, one can see that the differences in the temperature fields induced by variable conductivity prevail globally in the mantle. We note that these cases were for heating characteristic of chondritic abundance and that in the Hadean and Archean ages the radiogenic heating is at least four–five

times greater. For a young earth there is also heat left over from the core formation (Keondjian and Monin, 1977), which can also interact strongly with variable thermal conductivity, especially in regions where  $\partial k/\partial T$  changes signs. Therefore, there would be great possibility for significant melting to take place in a young mantle as a consequence of various feedback mechanisms, leading to both mechanical and chemical separation of the radiogenic materials in a magma ocean (e.g. Hofmeister (1983)), earlier pressure-melting in the Archean (Vlaar et al., 1994) and their subsequent rapid ascent to the crust (Bartlett, 1969; Carlson, 1994). Thus, the variable conductivity model would predict an initial depletion of the radiogenic elements in the lower mantle by the melting episodes, since it is well accepted that the vertical transport of melt migration by solitary waves is a very efficient process (Scott and Stevenson, 1984; Scott et al., 1986) much more so than by ordinary viscous flow in mantle convection (Schmelting, 2000).

Alternatively, in the case of a more gradually overheated lower mantle, this positive feedback process could also cause occasionally large gushing events involving the outpour of hot lower mantle material through the endothermic phase transitional barrier established regionally or globally at the 660 km boundary by the vigor of high surface Rayleigh number convection (Yuen et al., 1998; Cserepes and Yuen, 2000). Such a scenario of layered mantle convection involving the upward gushing of hot lower mantle material through the endothermic phase transition and subsequent lithospheric resurfacing was first suggested for a hot Venusian mantle by Steinbach and Yuen (1992) and also in the earth's mantle by Yuen et al. (1998).

### 4.2. Delayed cooling of the mantle

The rate of cooling of the mantle is crucial in determining the thermal evolution of planetary interiors and the usual assumption of quasi-static cooling is made in which the heat transfer at each time step is similar to the steady-state value (Schubert et al., 1980). Our results for secular cooling with an adiabatic core-mantle boundary and time-dependent internal heating show that the cooling rates are slower for variable conductivity models because of the feedback between internal heating and variable conductivity.

Thus, the hot lower mantle model recently proposed by Kellogg et al. (1999) may possibly be explained by the higher lower mantle temperature caused by variable thermal conductivity (Dubuffet et al., 1999). In this connection the thermal assimilation of cold slabs in the bottom third of the lower mantle can also be explained by variable thermal conductivity due to the higher thermal conductivity in colder environments (Dubuffet et al., 2000). Therefore, variable thermal conductivity with some amounts of internal heating can account also for many predictions set forth by the recent model in which the lower mantle is currently both hot and chemically stratified (Kellogg et al., 1999).

Hansen and Yuen (2000) using a variable viscosity model found that there is overheating in the lower mantle in thermal-chemical convection models with variable viscosity, internal heating of chondritic abundance and mechanical heating such as adiabatic and viscous dissipation terms included. But constant thermal conductivity was employed in the work of Hansen and Yuen (2000), who have tested the Kellogg model against more realistic thermal-chemical convection model with viscous and adiabatic heating included. Thus, there would be even more severe overheating in the thermal-chemical convection model of (Hansen and Yuen, 2000) with variable thermal conductivity, which would possibly lead to wholesale melting today in the deep lower mantle. From these arguments, we may conclude that if the lower mantle is indeed chemically stratified, then it would be extremely difficult not to find some amounts of melting in the lower mantle today in the presence of variable mantle thermal conductivity.

In this work we have presented sufficient evidence from two-dimensional numerical modeling to show that there is a definite need for including realistic thermal conductivity in modeling the thermal evolution of the mantle, because the thermal consequences are not negligible at all and can cause severe consequences for deep-seated melting and the transport of melt volatiles from the lower to upper mantle (Gasparik and Hutchinson, 2000). We anticipate that three-dimensional modeling will essentially capture the same physics, based on our previous experience with comparing two-dimensional and three-dimensional results (Dubuffet et al., 2000). The effects of variable viscosity with both pressure- and temperature-

dependence would be examined next because of its importance on questions regarding melting in the deep mantle with enriched radioactivity (Kellogg et al., 1999).

## Acknowledgements

We thank the discussions with Drs. Fabien Dubuffet and Anne Hofmeister. Support of this research has come from the geophysics program of the National Science Foundation.

## Appendix A. PC time integration of the non-linear energy equations

The time integration scheme for the non-linear equations consists of the following steps:

$$\begin{aligned} \Delta t^{-1} M \left[ T_0^{(n+1)} - T^{(n)} \right] - A(T^{(n)}, U^{(n)}) T_0^{(n+1)} \\ = G(U^{(n)}) \end{aligned} \quad (\text{A.1})$$

Eq. (A.1) is solved for the predictor temperature vector  $T_0^{(n+1)}$ , in terms of the known temperature  $T_n$  for  $t = t_n$ .

$$S U_0^{(n+1)} = F(T_0^{(n+1)}) \quad (\text{A.2})$$

Eq. (A.2) is solved for the predictor velocity vector  $U_0^{(n+1)}$ .

The predictor temperature and velocity can then be used as starting values for the iterative Crank–Nicolson multi-corrector

$$\begin{aligned} \Delta t^{-1} M [T_{j+1}^{(n+1)} - T^{(n)}] + \frac{1}{2} A(T_j^{(n+1)}, U_j^{(n+1)}) T_{j+1}^{(n+1)} \\ + \frac{1}{2} A(T^{(n)}, U^{(n)}) T^{(n)} = \frac{1}{2} G(U_j^{(n+1)}) + \frac{1}{2} G(U^{(n)}) \end{aligned} \quad (\text{A.3})$$

$$S U_{j+1}^{(n+1)} = F(T_{j+1}^{(n+1)}) \quad (\text{A.4})$$

Eqs. (A.3) and (A.4) are solved in that order in a recursion  $j = 1, 2, \dots$  for  $T_{j+1}^{(n+1)}, U_{j+1}^{(n+1)}$  where the recursion is started from the predictor vectors  $T_0^{(n+1)}, U_0^{(n+1)}$  and the recursion in  $j$  is stopped when a convergence criterion  $\max[\epsilon_T, \epsilon_U] < \epsilon$  is

satisfied, where

$$\epsilon_T = \frac{\|T_{j+1}^{(n+1)} - T_j^{(n+1)}\|}{\|T_{j+1}^{(n+1)}\|},$$

$$\epsilon_U = \frac{\|U_{j+1}^{(n+1)} - U_j^{(n+1)}\|}{\|U_{j+1}^{(n+1)}\|} \quad (\text{A.5})$$

The problem is non-linear due to the temperature-dependence in  $k(T, P)$  which makes the matrix  $A$  dependent on the solution vector  $T$ . The multi-corrector scheme implies a similar Picard iteration, as used commonly for solving the non-linear Stokes equation in model cases with non-linear rheology (van den Berg et al., 1993).

## References

- Balachandar, S., Yuen, D.A., Reuteler, D., 1993. Viscous and adiabatic heating effects in three-dimensional compressible convection at infinite Prandtl number. *Phys. Fluids* 5 (11), 2938–2945.
- Barenblatt, G.I., Zel'dovich, Y.B., 1972. Self-similar solutions as intermediate asymptotics. *Ann. Rev. Fluid Mech.* 4, 285–312.
- Barenblatt, G.I., 1996. *Scaling, Self-Similarity, and Intermediate Asymptotics*, Cambridge University Press, Cambridge, 386, pp. 1996.
- Bartlett, R.W., 1969. Magma convection, temperature distribution, and differentiation. *Am. J. Sci.* 267, 1067–1082.
- Branlund, J., Kameyama, M.C., Yuen, D.A., Kaneda, Y., 2000. Effects of temperature-dependent thermal diffusivity on shear instability in a viscoelastic zone: implication for faster ductile faulting and earthquakes in the spinel stability field. *Earth Planet. Sci. Lett.* 182 (2), 171–185.
- Brown, J.M., 1986. Interpretation of the D'' zone at the base of the mantle: dependence on assumed values of thermal conductivity. *Geophys. Res. Lett.* 13, 1509–1512.
- Carlson, R.W., 1994. Mechanisms of earth differentiation: consequences for the chemical structure of the mantle. *Rev. Geophys.* 32, 337–361.
- Chopelas, A., Boehler, R., 1992. Thermal expansivity of the lower mantle. *Geophys. Res. Lett.* 19, 1983–1986.
- Choblet, G., Sotin, C., 2000. 3D thermal convection with variable viscosity: can transient cooling be described by a quasi-static scaling law. *Phys. Earth Planet. Int.* 119, 321–336.
- Christensen, U.R., Yuen, D.A., 1985. Layered convection induced by phase transitions. *J. Geophys. Res.* 90, 10291–10300.
- Cserepes, L., Yuen, D.A., 2000. On the possibility of a second kind of mantle plume. *Earth Planet. Sci. Lett.* 183, 61–71.
- Daly, S.F., 1980. Convection with decaying heat sources: constant viscosity. *Geophys. J. R. Astron. Cos.* 61, 519–547.
- DeLandro-Clarke, W., Jarvis, G.T., 1997. Numerical models of mantle convection with secular cooling. *Geophys. J. Int.* 129, 183–193.
- Dubuffet, F., Yuen, D.A., Rabinowicz, M., 1999. Effects of a realistic mantle thermal conductivity on the patterns of three-dimensional convection. *Earth Planet. Sci. Lett.* 171, 401–409.
- Dubuffet, F., Yuen, D.A., 2000. A thick pipe-like heat-transfer mechanism in the mantle: non-linear coupling between three-dimensional convection and variable thermal conductivity. *Geophys. Res. Lett.* 27 (1), 17–20.
- Dubuffet, F., Yuen, D.A., Yanagawa, T., 2000. Feedback effects of variable thermal conductivity on the cold downwellings in high surface Rayleigh number convection. *Geophys. Res. Lett.* 27 (18), 2981–2984.
- Gasparik, T., Hutchinson, M.T., 2000. Experimental evidence for the origin of two kinds of inclusions in diamonds from the deep mantle. *Earth Planet. Sci. Lett.* 181, 103–114.
- Hansen, U., Yuen, D.A., Kroening, S.E., Larsen, T.B., 1993. Dynamical consequences of depth-dependent thermal expansivity and viscosity on mantle circulations and thermal structure. *Phys. Earth. Planet. Int.* 77, 205–223.
- Hansen, U., Yuen, D.A., 2000. Extended-Boussinesq thermal-chemical convection with moving heat sources and variable viscosity. *Earth Planet. Sci. Lett.* 176, 401–411.
- Hauck, S.A., Phillips, R.J., Hofmeister, A.M., 1999. Variable conductivity: effects on the thermal structure of subducting slabs. *Geophys. Res. Lett.* 26 (2), 3257–3260.
- Hofmeister, A.M., 1983. Effect of a hadean terrestrial magma ocean on crust and mantle evolution. *J. Geophys. Res.* 88, 4963–4983.
- Hofmeister, A.M., 1999. Mantle values of thermal conductivity and the geotherm from phonon lifetimes. *Science* 283, 1699–1706.
- Honda, S., Yuen, D.A., 2001. Interplay of variable thermal conductivity and expansivity on the thermal structure of the oceanic lithosphere. *Geophys. Res. Lett.* 28 (2), 351–354.
- Hughes, T.J.R., 1987. *The Finite Element Method: Linear Static and Dynamic Finite Element Analysis*, Prentice Hall, Englewood Cliffs, NJ, 1987, 803 pp.
- Ita, J., King, S.D., 1994. Sensitivity of convection with an endothermic phase change to the form of the governing equations, initial conditions, boundary conditions, and equation of state. *J. Geophys. Res.* 99, 15919–15938.
- Kellogg, L.H., Hager, B.H., van der Hilst, R.D., 1999. Compositional stratification in the deep mantle. *Science* 283, 1881–1884.
- Keondjian, V.P., Monin, A.S., 1977. Calculations of the evolution of the planetary interiors. *Tectonophysics* 41, 227–242.
- Klemens, P., 1958. Thermal conductivity and lattice vibration modes. In: Seitz, F., Turnbull, D. (Eds.), Vol. 7, *Solid State Physics*, Academic Press, New York, pp. 1–98.
- Leitch, A.M., Yuen, D.A., 1989. Internal heating and thermal constraints on the mantle. *Geophys. Res. Lett.* 16, 1407–1410.
- Leitch, A.M., 1995. Effects of temperature and mantle dynamics on estimates of the thermal conductivity in the deep mantle. *Phys. Earth Planet. Int.* 89, 89–108.
- Lubimova, A.H., 1958. Thermal history of the earth with consideration of the variable thermal conductivity of the mantle. *Geophys. J.R. Astr. Sco.* 1, 115–134.
- Machel, P., Yuen, D.A., 1989. Penetrative convective flows induced by internal heating and mantle compressibility. *J. Geophys. Res.* 94, 10609–10626.

- Mac Donald, G.J.F., 1959. Calculations on the thermal history of the earth. *J. Geophys. Res.* 64, 1967–2000.
- Manga, M., Jeanloz, R., 1996. Implications of a metal-bearing chemical boundary layer in D'' for mantle dynamics. *Geophys. Res. Lett.* 23 (22), 3091–3094.
- Matyska, C., Moser, J., Yuen, D.A., 1994. The potential influence of radiative heat transfer on the formation of megaplumes in the lower mantle. *Earth Planet. Sci. Lett.* 125, 255–266.
- Parsons, B., Sclater, J.G., 1977. An analysis of the variation of the ocean floor bathymetry and heat flow with age. *J. Geophys. Res.* 82, 803–827.
- Quarení, F., Yuen, D.A., Sewell, G., Christensen, U.R., 1985. Mean-field convection solutions for strongly variable viscosity and high surface Rayleigh numbers: a comparison with two-dimensional solutions. *J. Geophys. Res.* 90, 12633–12644.
- Ross, R.G., Andersson, P., Sundqvist, B., Backstrom, G., 1984. Thermal conductivity of solids and liquids under pressure. *Rep. Prog. Phys.* 47, 1347–1402.
- Schmeling, H., 2000. Partial melting and melt segregation in a convecting mantle. In: Bagdassarov, N., Laporte, D., Thompson, A.B. (Eds.), *Physics and Chemistry of Partially Molten Rocks*, Kluwer Academic Publishers, Dordrecht, pp. 141–178.
- Schubert, G., Stevenson, D., Cassen, P., 1980. Whole planet cooling and the radiogenic heat source content of the earth and moon. *J. Geophys. Res.* 85, 2531–2538.
- Scott, D.R., Stevenson, D.J., 1984. Magma solitons. *Geophys. Res. Lett.* 11, 1161–1164.
- Scott, D.R., Stevenson, J., Whitehead, J.A., 1986. Observations of solitary waves in a viscously deformable pipe. *Nature* 319, 759–761.
- Shankland, T.J., Nitsan, U., Duba, A.G., 1979. Optical absorption and radiative heat transport in olivine at high temperature. *J. Geophys. Res.* 84 (B4), 1603–1610.
- Siegel, R., Howell, J.R., 1972. *Thermal Radiation Heat Transfer*, McGraw-Hill, New York, 1972.
- Starin, L., Yuen, D.A., Bergeron, S.Y., 2000. Thermal evolution of sedimentary basin formation with temperature-dependent conductivity. *Geophys. Res. Lett.* 27 (2), 265–268.
- Steinbach, V., Hansen, U., Ebel, A., 1989. Compressible convection in the earth's mantle: a comparison of different approaches. *Geophys. Res. Lett.* 16, 633–635.
- Steinbach, V., Yuen, D.A., 1992. The Effects of multiple phase transitions on Venusian mantle convection. *Geophys. Res. Lett.* 19, 2243–2246.
- Steinbach, V., Yuen, D.A., Zhao, W., 1993. Instabilities from phase transitions and the timescales of mantle evolution. *Geophys. Res. Lett.* 20, 1119–1122.
- van den Berg, A.P., van Keken, P.E., Yuen, D.A., 1993. The effects of a composite non-Newtonian and Newtonian rheology in mantle convection. *Geophys. J. Int.* 115, 62–78.
- van den Berg, A.P., Yuen, D.A., 1998. Modeling planetary dynamics by using the temperature at the core-mantle boundary as a control variable: effects of rheological layering on mantle heat transport. *Phys. Earth Planet. Int.* 108, 219–234.
- van den Berg, A.P., Yuen, D.A., Steinbach, V., 2001. The effects of variable thermal conductivity on mantle heat-transfer. *Geophys. Res. Lett.* 28 (5), 875–878.
- Vlaar, N.J., van Keken, P.E., van den Berg, A.P., 1994. Cooling of the earth in the Archaean: consequences of pressure-release melting in a hotter mantle. *Earth Planet. Sci. Lett.* 121, 1–18.
- Weertman, J., 1970. The creep strength of the earth's mantle. *Rev. Geophys. Space Phys.* 8, 145–168.
- Zhang, S., Yuen, D.A., 1996. Various influences on plumes and dynamics in time-dependent, compressible, mantle convection in three-dimensional spherical shell. *Phys. Earth Planet. Int.* 94, 241–267.
- Yuen, D.A., Cserepes, L., Schroeder, B.A., 1998. Mesoscale structures in the transition zone: dynamical consequences of boundary layer activities. *Earth Planets Space* 50, 1035–1045.